AAPS PharmSciTech (2019) 20: 271
DOI: 10.1208/s12249-019-1482-0

Review Article

Theme: Paul Myrdal Memorial Issue - Pharmaceutical Formulation and Aerosol Sciences
Guest Editors: Philip J. Kuehl and Stephen W. Stein

Effect of Roughness on the Dispersion of Dry Powders for Inhalation: a Dynamic Visualization Perspective

Xiang Kou,[1,2] Paul W. S. Heng,[1] Lai Wah Chan,[1] Steven T. Wereley,[3] and M. Teresa Carvajal[2,4]

Received 10 January 2019; accepted 12 July 2019; published online 30 July 2019

Abstract. Dry powder inhalers have attracted more interest over the years in every aspect related to them. Interestingly, when focusing on the effects of particle morphology of the active or carrier (excipient), it is generally regarded particle size and shape to influence drug availability of aerosolized particles. However, to date, few studies have examined the effect of texture, *i.e.*, roughness, on this relationship. The main objective of the present work is to gain a closer understanding of the influence of carrier morphology on the aerosolization performance of dry powder inhaler formulations. Image analysis and microscopy were used to visualize the aerosolization process. It is considered that the scale of morphological features on the surface of the carrier particles is responsible for the dispersion of the powder formulation, separation of the drug/carrier, and entrainment from a dry powder inhaler. Thus, for this study, the carrier particles of different surface roughness were mixed with micronized salbutamol sulphate. Aerosolization *in vitro* testing was used to evaluate the performance. The results indicate a connection between the qualitative surface roughness of coarse carriers and aerosolization performance during powder dispersibility. This investigation demonstrated that indeed, powder dispersion, a dynamic process, is influenced by the scale of the carrier morphology.

KEY WORDS: dry powder inhalers; particle morphology; roughness; particle surface energy; image analysis.

INTRODUCTION

Dry powder inhalers (DPIs) are an alternative drug delivery method for the treatment of various lung diseases. DPIs offer unique advantages, making them suitable for both small and large molecules (1,2). The DPI formulations are generally composed of dry powder blends of active pharmaceutical ingredient (API) and a coarse carrier. Also, DPIs are widely recognized that the morphology of the coarse carrier plays an important role in the agglomeration/de-agglomeration properties of DPIs (3–8). Numerous efforts for improving formulation performance are focused on manipulating the texture of the coarse carrier excipient. The studies include changing surface roughness by spray drying (9), recrystallization (6), precision coating (10), or mechanofusion (11). The majority of the studies of this nature have been on trial-and-error basis. This leads to a wide variety of roughness in which the mechanism of dispersion is unclear. A better understanding of the roughness effect on dry powder dispersion mechanism is necessary to guide product design at various steps of the formulation, processing, stability, and performance. This work addresses the dispersion mechanism from the visualization and qualitative perspective, whereas the functionality and performance from the quantitative *in vitro* testing.

Some studies have reported that an increase in roughness leads to a decrease in fine particle fraction (FPF), likely due to multiple contact points between the drug and the carrier. An increase in contact points favors binding and consequently an increase in drug adhesion to the carrier (12,13). Similarly, increasing the interlocking propensity and frictional forces between the particles (12,14) leads to a lower FPF. Interestingly, conflicting results have been reported (4,7,14–21) for lactose and for mannitol-based carriers (22) where findings have been attributed to the existence of various levels of roughness (23). It should be noticed that roughness studies that have a similar adhesion force does not guarantee a similar aerodynamic behavior of the drug in the cascade

Guest Editors: Philip J. Kuehl and Stephen W. Stein

[1] National University of Singapore, 21 Lower Kent Ridge Rd, Singapore, Singapore.
[2] Agricultural and Biological Engineering, Purdue University, West Lafayette, Indiana, USA.
[3] Mechanical Engineering, Purdue University, West Lafayette, Indiana, USA.
[4] To whom correspondence should be addressed. (e–mail: tcarvaja@purdue.edu)

impactor (24), because the roughness effect on the dispersion also depends on how particles are dispersed (6). This explanation still does not reconcile the fact that roughness cannot predict the in vitro performance (24). Thus, a static measurement parameter is not capable of reflecting a dynamic process. The dispersion phenomenon from dry powders for inhalation devices might be attributed to the dynamic nature of the process.

Few reports in the literature have investigated through modeling the dynamic aspects of the powder dispersion phenomena. Those studies propose that the drug detachment and dispersion processes from carrier particles are due to two major detachment mechanisms: by the flow stream (fluid forces) and by impaction (mechanical forces) (25,26), suggesting an increased incidence of collisions the aerosol performance improves (27–29). Thus, based on the results of modeling, this study considers experimental observation of the forces involved in the drug detachment mechanism and proposes shifts from flow-based to impaction-based as the carrier roughness increases.

This study provides direct experimental observation using image analysis to address the dispersion process and to investigate the roughness effect on the dispersion process. The resulting observations lead to the identification, degree and extent of the parameters governing dispersion.

EXPERIMENTAL

Materials

Salbutamol sulfate (Fine drugs and chemicals, Hyderabad, India) was used as a model drug. Micronized salbutamol sulfate (MSS) was obtained using a fluidized bed opposed jet mill (AFG 100, Hosokawa, Augsburg, Germany) at a pressure of 4 bar and a classifier wheel speed of 15,000 rpm. Air-sieved coarse carrier (ASCC) was obtained by air jet sieving Pharmatose 450M (DMV, Veghel, The Netherlands) in the range of 44–63 μm, noted as ASCC. Micronized lactose was obtained by jet milling Pharmatose 200M at a pressure of 4 bar and a classifier wheel speed of 15,000 rpm; the resulting material was denoted as fines.

Roughness-modulated coarse carriers (RMCCs) were obtained by first roller compacting (Hosokawa Bepex, GmbH, Germany) Pharmatose 200M, followed by using several unit operations in the sequence of sieving, cone milling, air jet milling, and sieving. The roller compaction conditions are shown in Table I. Flakes produced by roller compaction were first sieved (1.0 mm aperture size; Retsch, Germany) to remove fine particles. The flakes without fine particles were placed in a cone milled (Model 197S, Quadro Engineering, Waterloo, Canada) using a 0.045-inch aperture size screen at impeller speed of 4000 rpm to produce granules, which were further comminuted by jet milling (Hosokawa, AFG 100, Augsburg, Germany) at a pressure of 4 bars and a classifier wheel speed of 2000 rpm. The resulting powder passed through air jet sieve in the range of 44–63 μm. The resulting material was denominated as surface roughness-modulated coarse carrier (RMCC).

Model Formulation Systems

Three different formulation systems (total of 7 model formulations) (Table II) were prepared: (1) neat micronized salbutamol sulfate (MSS). Neat micronized salbutamol sulfate (MSS) is rarely used alone as formulation. However, due to its inexplicit and uncertain behavior, it was used as a control group; (2) binary mixture of micronized salbutamol sulfate (MSS) and coarse carriers in which two types of coarse carriers ASCC and RMCCs were used; model binary mixtures include ASCC with MSS and four different RMCCs with MSS; and (3) ternary mixture of micronized salbutamol sulfate (MSS) with a mixture of ASCC and 10% fines.

For the binary mixture, micronized salbutamol sulfate (MSS) was mixed with coarse carrier (either ASCC or RMCC) in a ratio of 1:67.5 (*w*/*w*). Four different RMCCs with different roller compaction process conditions were used. A portion of the coarse carrier is weighed into a 20-mL sample vial containing the MSS. The vial was closed with a stopper and the contents blended using a Vortex mixer for 5 s. More coarse carriers are added into the vial and blended. This process was repeated until all the coarse carriers have been incorporated. The whole mixture was finally blended for another 10 min to offset any mixing order sequence effect.

For the preparation of the ternary mixture, binary mixture of ASCC with 10% lactose fines was first prepared then a portion of ASCC is mixed with fines. The vial was closed with a stopper and the contents blended using a Vortex mixer for 5 s. More ASCC powder was added into the vial and blended again. This process was repeated until all the ASCC materials have been incorporated. The whole binary mixture of ASCC and lactose fines was finally blended for another 10 min to offset any mixing order sequence effect. Micronized salbutamol sulfate (MSS) was then blended with

Table I. Roller Compaction Processing Condition

Group	Roller speed (rpm)	Screw speed (rpm)	Compression force (kN)
RC 1	2.6	30	60
RC 2	2.6	40	80
RC 3	2.6	45	100
RC 4	2.6	50	125

The air jet milled powder from roller compacted granule is denoted as RMCC1, RMCC2, RMCC3, RMCC4

Table II. Model Formulation Composition

Model formulation	Carrier type	Micronized salbutamol sulfate percentage
1	–	100%
2	ASCC	1.45%
3	ASCC+10% Fines	1.45%
4	RMCC1	1.45%
5	RMCC2	1.45%
6	RMCC3	1.45%
7	RMCC4	1.45%

the above mixture in a ratio of 1:67.5 (*w*/*w*) to obtain the final ternary mixture.

Filling of Capsules

Hard gelatin capsules (size 3) were filled with 30.0 ± 1.5 mg each of the 7 model formulations. The capsules were filled manually in a controlled environment at 25 °C and 50 % relative humidity.

Particle Size Determination

Particle size was determined using a laser diffraction particle size analyzer (Coulter LS 230, Coulter Corporation, Hialeah, FL, USA), equipped with a small volume module. The powder sample was suspended in hexane sonicated for 30 s to break the agglomerates before measurement following procedures as conducted in other study (30). The Dv50 of the sample was determined.

Surface Morphology

Surface morphology was determined by SEM. The particles were gold-sputter-coated under a vacuum before viewing under the SEM (JSM-5200, JEOL, Japan). Photomicrographs of the particles were obtained using image capture software (SemAfore, Version 4.02, Finland).

Roughness Measurement

Around 60 particles were randomly selected for each coarse carrier system (RMCCs and ASCC). Particles were scanned using an optical profiler (Wyko NT1100, Veeco, USA) under a field of view of 109.7 μm × 144.1 μm. The roughness average (Ra) was calculated for each sample using the height profile obtained from the AFM instrument. Therefore, Ra is the arithmetic mean of the absolute values of the height of the surface profile. Surface roughness of single particle was quantified using the arithmetic mean roughness (Ra) calculated from an area of 20 μm × 20 μm using Vision 3.0 software (Veeco, USA). Ra was calculated as $Ra = \frac{1}{L}\int_0^L \{f(x)\}dx$, where L is the evaluation length and f(x) is the profile height function that measures each individual height relative to the base line. A higher Ra value indicates a rougher surface.

Surface Energy Measurement

Inverse gas chromatography (iGC 2000, Surface Measurement Systems Ltd, UK) was used to assess the surface energetics of the coarse carriers. Approximately 1 g of sample was packed in a siliconized glass column using a standardized tapping method; glass wool was placed in both ends of the column. A linear series of alkanes (heptane, octane, nonane, and decane) was the non-polar probes for the determination of dispersive surface energy of the sample. The probes were injected at infinite dilution at 303 K and measured using a flame ionization detector (FID). The dispersive surface energy was calculated according to the method by Schultz et al. (31). All samples were tested in triplicates.

In Vitro Aerosolization Characterization

Formulations were aerosolized from 30 mg capsules (size 3, gelatin) using a Rotahaler at 30 L min^{-1} into a Next Generation Impactor (NGI, MSP Corporation, Minnesota, USA) with a USP throat inlet and pre-separator. The *in vitro* deposition test was repeated for five capsules. Then, the impactor was dismantled; the mouth piece, throat, pre-separator, and individual plates were carefully washed with the mobile phase used for the HPLC analysis. The concentrations of salbutamol sulfate on each of the collection plate were determined by high-performance liquid chromatography (HPLC, Shimadzu 2010, Shimadzu, Japan). The mobile phase was composed of 45: 55 (*v*/*v*) of methanol and 0.2% (*w*/*v*) aqueous ammonium acetate at a flow rate of 0.5 mL/min, equipped with an ultraviolet spectrophotometry (UV) detector set at 276 nm for the detection of the drug. The experiments were carried out in triplicate ($n = 3$). A calibration curve for salbutamol sulfate was obtained: $y = 67423x - 11865$ ($R^2 = 0.9997$), where y is the integrated area under the HPLC curve, and x is the drug content. The drug content released from the device and deposited in different stages in the impactor. Fine particle fraction (FPF) is defined the mass fraction of drug particles smaller than 5 micron recovered from stage 3 to filter (32).

Dry Powder Dispersion in Inhaler Chamber Real-Time Visualization

A transparent tube was constructed according to the Rotahaler's configuration to mimic the inhaler device (Fig. 1). Ten samples from each model formulation were used for the dispersion visualization study. The samples were aerosolized into the transparent model inhaler for visualization purposes followed by using a next-generation impactor (MSP Corporation, MN, USA) at 30 L/min. The aerosolization is induced by a vacuum pump connected to the next-generation impactor. A camera lens was fitted to a high-speed camera (Hotshot 512 SC, NAC Image Technology Inc, USA) for visualization of the powder dispersion process. A light source (Nikon Intenslight C-HGFI) illuminated the image capture field. The aerosolization process was visualized from side view.

The video recording started when the vacuum pump was switched on. The images were captured and analyzed using a self-written software (EDPIV). At least 1000 particles were

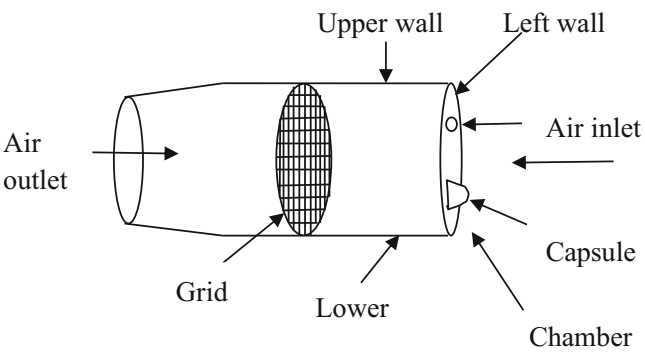

Fig. 1. Schematic diagram of the inhaler device

Table III. Particle Size

Sample	Dv(50) (μm)
Micronized salbutamol sulfate (MSS)	1.8 ± 0.9
Fines	3.6 ± 0.9
Air sieved coarse carrier (ASCC)	42.6 ± 3.3
Air sieved coarse carrier+10% fines	48.2 ± 1.2
RMCC1	39.5 ± 6.3
RMCC2	36.5 ± 4.1
RMCC3	34.4 ± 10.9
RMCC4	42.3 ± 4.9

Values after ± represent standard deviation

analyzed on each image. Particles were identified and tracked manually. Both software analysis data and manual tracking data were used for further analysis. Manual particle tracking was used to validate the data calculated by the software. The collision number, particle velocities, velocity difference, median velocity, velocity change after collision, and total energy exchange during collisions were calculated. The collision number is the cumulative number of occurrence for particle-particle and particle-device collision at a certain period. Particle velocities were determined based on the distance the particles have to travel in consequential images and the time interval. A pool of velocities at each time point for each model formulation was then established. The velocity difference is the difference between the largest velocity and smallest velocity; the median velocity is the 50th percentile of the cumulative velocity plot; the velocity change is the absolute difference before and after collision and the total energy exchange during collision is calculated according to the following equation:

$$\text{Energy} = \text{collision number} * \frac{1}{2} m \Delta v^2, m = \rho \frac{1}{6} \pi d^3 \quad (1)$$

where m is the mass, ρ is the density (1.55 g/cm^3 for lactose as reported (33)), d is the particle's diameter, ,Δv is the velocity change, and $\frac{1}{2} m \Delta v^2$ is the energy input for each collision.

Particle Image Velocimetry Measurement Validation

Particle image velocimetry measurement was firstly validated prior to the analysis of the images captured. The validation consisted in comparing the velocities calculated by the software and the manual particle tracking and by calculating the root-mean-square deviation (RMSD) where a smaller RMSD indicates a good fit.

RESULTS AND DISCUSSION

Particle Size and Surface Morphology of the Materials

Table III displays the particle size (p.s.) of materials; micronized salbutamol sulfate (MSS) and fines are all in the range of 1–5 μm, a typical particle size range obtained by air jet milling for pulmonary drug delivery. The mixture of ASCC with 10% of fines has larger size (48.2 μm) compared to that of ASCC

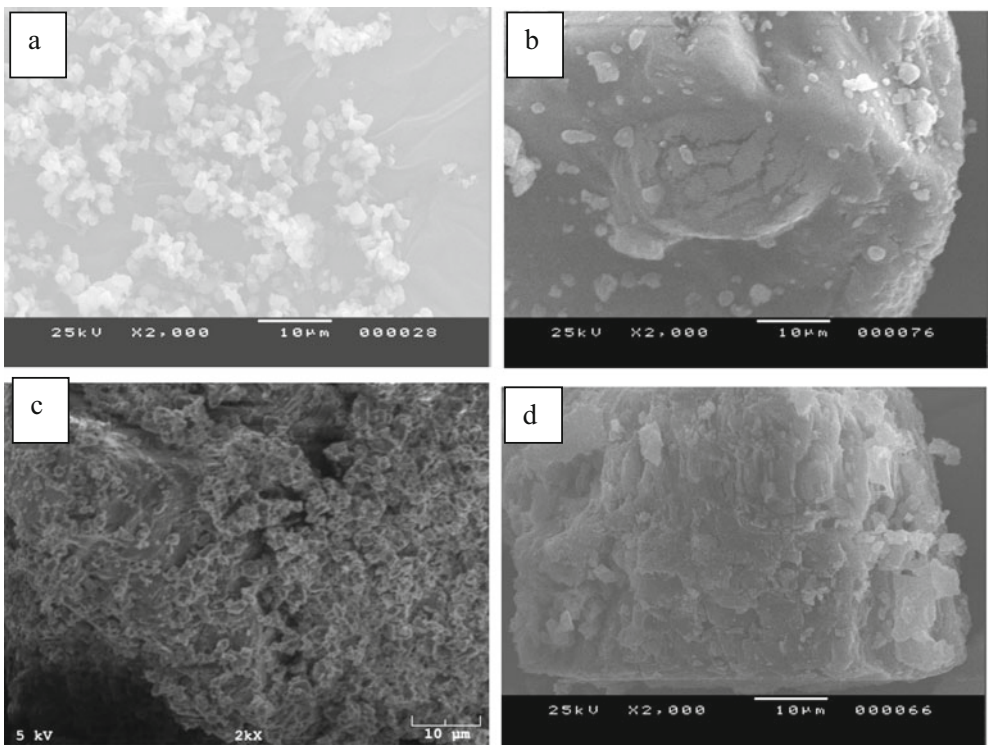

Fig. 2. SEM photomicrographs. **a** Micronized salbutamol sulfate (MSS). **b** Air jet sieved coarse lactose carrier (ASCC). **c** Binary mixture of air jet sieved coarse carrier (ASCC) with 10% fines. **d** Roughness-modulated coarse carrier 3 (RMCC3)

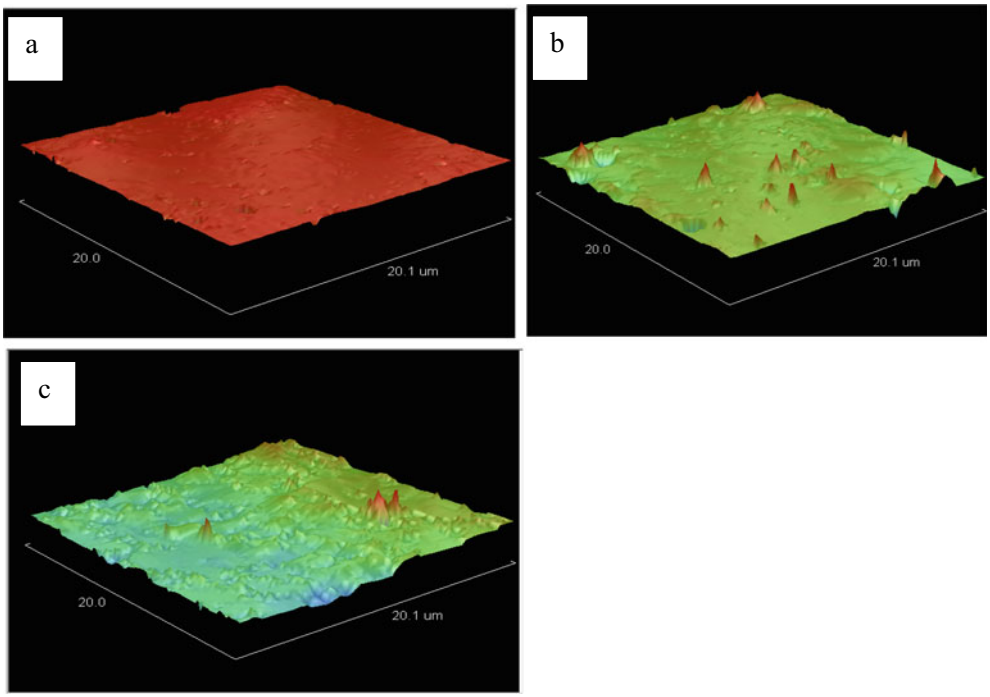

Fig. 3. Surface morphology of carriers. **a** Air sieved coarse carrier (ASCC). **b** Binary mixture of ASCC with 10% lactose fines. **c** Roughness-modulated coarse carrier 3 (RMCC3)

alone (42.6 μm). This suggests that the particles denominated as fines adhere to the outer layer of ASCC as displayed in Fig. 2c, which seems to indicate that the particle size is larger. On the other hand, the coarse carriers (RMCCs) with modulated roughness are in the range of 20–45 μm.

Neat micronized salbutamol sulfate (MSS) formed agglomerates due to its smaller size (Fig. 2a) whereas air jet-sieved coarse carrier (ASCC) seemed to have a smoother-like surface with few smaller particles left on its surface (Fig. 2b). The SEM images depicted in Fig. 2c and d indicated that fines led to agglomeration or clusters when covering the surface of ASCC in the binary mixture of ASCC and fines while the surface of RMCC seems to have some rugosity (Fig. 2d).

Roughness Measurement

The images for the surface morphology are displayed in Fig. 3. The air-sieved coarse carrier (ASCC) (Fig. 3a) looks smoother compared to the other two images (Fig. 3b and c). The particles in the binary mixture of ASCC and 10% fines appear to make changes on the surface as observed in Fig. 3b. Some lumps or protrusions are obvious, and it seems those are the agglomerated fines spotted in Fig. 2c. The images suggested that all the RMCC surfaces have uneven morphology surfaces, and this may be attributed to the lump-like appearance which may have been resulted in roughness (Fig. 3c).

The Ra values for roughness allow obtaining descriptors of powder behavior. The Ra numbers for the various carrier systems (from Table II) suggested that some samples are rougher than others. The images from Figs. 2c and 3b support the results obtained in Fig. 4 for these systems. Furthermore, the roller compaction processes, at various operating conditions, resulted on diverse roughness for the RMCC samples as revealed in Fig. 4. A total of 60 particles for each carrier system were used; 10 spots on each particle were tested. Thus, a total of 60 * 10 = 600 individual testing results were generated.

The variability of roughness could be attributed to the attrition and fragmentation during the roller compaction process (34,35). The data suggested that the highest roughness was obtained when the screw speed and compression force were at the highest values.

It is worth to note that the height is not the only parameter that influences the adhesion but also the contact points which are related to the spacing between nanoscale asperities. However, the scale assumed herein is at the microscale, such that it is possible to bring particle scale properties into descriptors of powder flow behavior. In this regard, a number of mechanisms have been proposed and reported wherein the complexities of real powder systems are treated as ideal powder systems comprised of round particles adhered into a flat surface; this has been done solely in an effort to simplify and start understanding powder systems. Likewise, in this study, in order to have insights of how the changes in rugosity affected the dispersion upon fluidization from a dynamic point of view using the visualization approach, roughness height is used. It is not suggested that

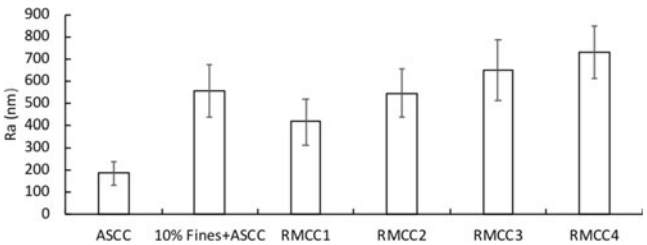

Fig. 4. Roughness of different carrier systems. The mean and standard deviation are calculated based on $n = 600$

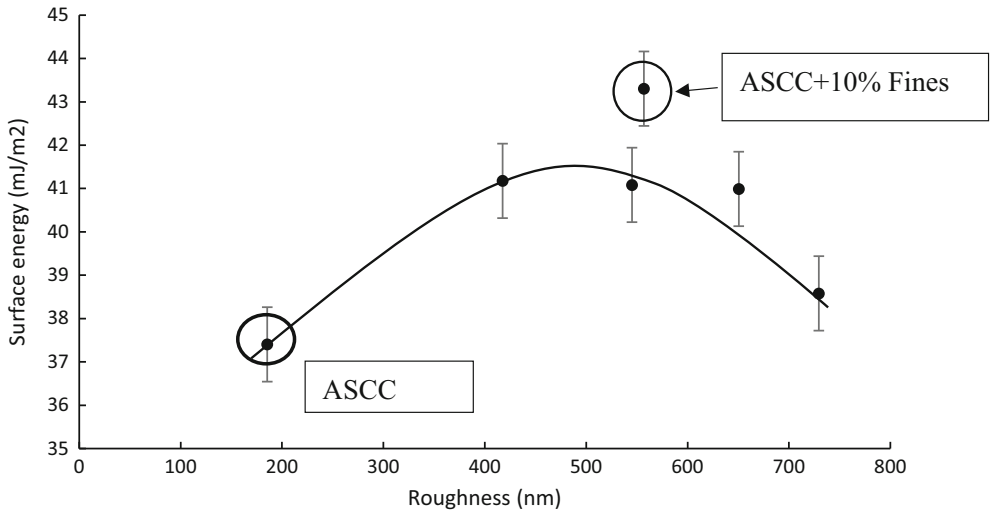

Fig. 5. Surface energy and surface roughness relationship for carriers ($n = 3$)

the roughness height is the only factor that influences adhesion, but due to limited evidence on deconvolution of all the confounding factors that influence an adhesion system, we propose a dynamic visualization approach and start building from there.

Surface Energetics Determination

Surface energetics has proven to be a good predictor of the interactions involved in the dispersion of powders for inhalation (36). It is conceivable to relate the dispersive component of the surface energy with the roughness of the powder systems as shown in Fig. 5 which suggests that for the contact geometry of the equivalent roughness between 400 and 600 nm, the surface energetics reaches a maximum. The data suggests that adding fine content to the coarse ASCC increases the cohesivity of the powders compared to the ASCC alone.

In Vitro Aerosolization Characterization

The *in vitro* results are plotted in Fig. 6. Neat micronized salbutamol sulfate (MSS) has very low FPF (formulation 1). This could be due to the cohesive nature of the MSS particles (37). MSS forms large and hard agglomerates that are difficult to break. In an effort to separate the very cohesive MSS particles, lactose is used improving the FPF as shown for formulations 2 (binary mixture of ASCC with MSS) and 3 (ternary mixture of ASCC, 10% lactose fines with MSS); these findings are in agreement with previous reports (38). As shown in the images collected during the fluidization experiments, formulations 2 and 3 can be dispersed by collision and drag forces (Fig. 7b). This leads to better *in vitro* results compared to formulation 1. Detailed dispersion process visualization and analysis for formulations 2 and 3 can be found elsewhere (39). The model formulations that consisted of RMCCs with MSS (Fig. 6, formulations 4–7) have an increase of FPF.

The *in vitro* results for different model formulations suggest that the effect of roughness on FPF cannot be explained solely by surface area change (40). The current notion is that a rougher surface is accompanied with fewer contact area points which leads to reduced inter-particulate adhesion forces. This enables easier detachment of drug from carrier surfaces during inhalation. Therefore, the formulation consisted of carrier excipients with rougher surfaces should have higher FPF and ED. However, this was not the case for model formulation 7 (binary mixture of MSS with the roughest RMCC) which has rougher carrier, with slightly declined FPF and ED. A higher roughness did not guarantee a higher FPF as reported elsewhere (24). The FPF results suggest that powder behavior (fluidization, dispersion or elutriation) is a complex dynamic process and cannot solely be explained due to roughness or presence of fines. Thus,

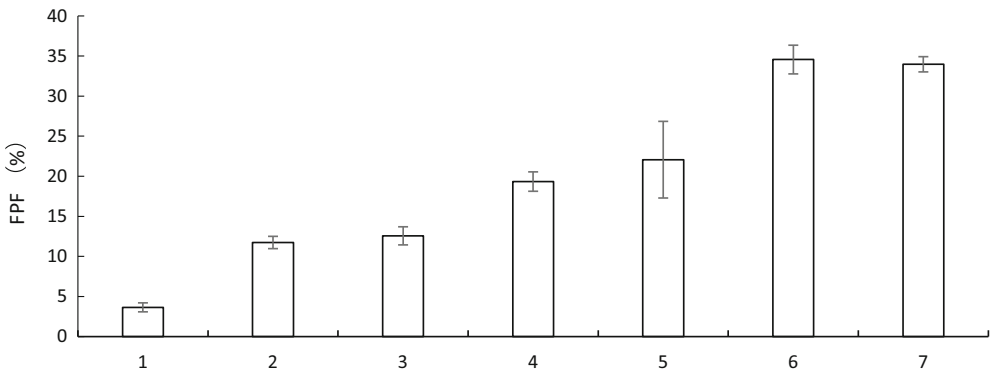

Fig. 6. *In vitro* aerosolization characterization of model formulations ($n = 5$)

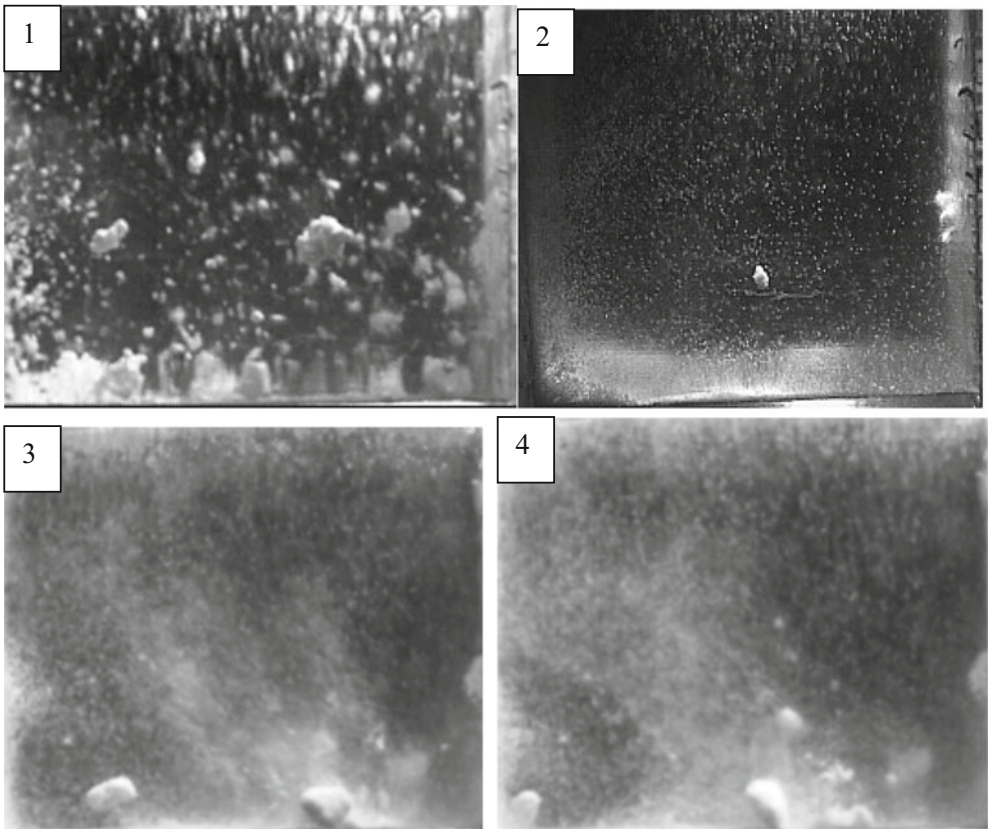

Fig. 7. Images of aerosolization process of **a** model formulation 1, **b** model formulation 3, and **c**, **d** model formulation 6. Time sequence is indicated by the label

dispersion should be investigated from a dynamic perspective. It is reasonable to believe that the energy exchange during collision and drag force are the major factors governing dispersion process.

Aerosolization Visualization

The aerosolization video captured the fluidization behavior as shown in Fig. 7. MSS formed large and hard agglomerates making it difficult to entrain the airstream; the drag force or collision was not high enough to break the agglomerates (Fig. 7a). Model formulations 2 and 3 were dispersed by both drag force and collision. A collision moment of model formulation 3 with obstacle is captured and shown in Fig. 7b. A detailed description of model formulations 1–3 aerosolization process is reported elsewhere (39). The powder in model formulations 4–7 forms loose agglomerates with good flowability. When the air is introduced, the agglomerates will be purged layer by layer. The number of particles suspended for RMCC model formulation in the air (Fig. 7c and d) is much more than other powder

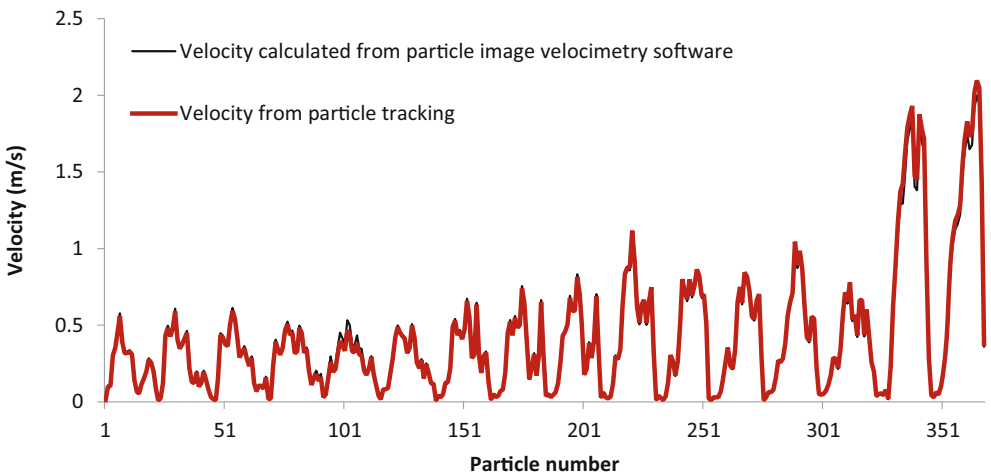

Fig. 8. Comparison of velocity obtained by automatic particle image velocimetry and manual particle tracking

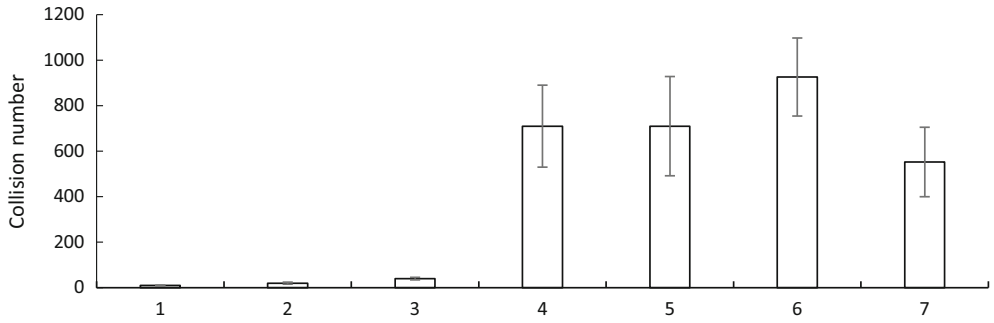

Fig. 9. Collision number for model formulations within the first 1 s of aerosolization, $n = 10$

systems (Fig. 7b). The loose agglomerates formed in RMCC formulations can be dispersed by drag force (Fig. 7c and d). During aerosolization, the powder is suspended within the device causing the particles to impact on the device. Single particles can also collide with each other due to its high population suspended in the air. Consequently, the existing mechanisms such as drag force, particle-obstacle impact, and particle-particle collisions contribute to affect the dispersion of the model RMCC formulations. The results suggest that the formulations consisted of RMCC have better *in vitro* results (Fig. 6) because the dispersion process was more efficient.

Particle Image Velocimetry Validation

The PIV system is validated by comparing the automatic and manual calculation (Fig. 8). The velocity values for automatic and manual calculations are equivalent. The RMSD is 0.02, which is 5% of the median velocity calculated using particle image velocimetry technique. This demonstrates that the automatic particle image velocimetry technique is accurate, reproducible, and robust for the particle velocity calculation in this study.

The following sections explain the phenomena through energy exchange perspective. Energy exchange is related to the total number of collisions and velocity change. It is worth to mention that in the following figures (Figs. 9, 10, 11, 12, and 13), approximately 1000 particles were analyzed for each of the image and roughly 15,000 images were collected per second for each model formulation to generate the data points.

Collision and Collision Number

The collision number and collision frequency are important factors in particle detachment and deagglomeration (41). Collisions in the dispersion of dry powders have two types: particle-particle collision and particle-obstacle collision. The collision number is one of the parameters to assess the collision process. The collision number for each model formulation was studied by tracking at least 1000 particles in each sample (10 samples per model formulation, ~ 70 samples). The collision number for the first 1 s for each sample was recorded as displayed in Fig. 9. Formulation 1 (MSS) had the lowest collision number. This could be attributed to the cohesiveness leading to the formation of strong agglomerates which do not follow the air stream and likely that the only collision is the impact of the large agglomerate with an obstacle within the device. In contrast, formulations 2 and 3 seem to have more collisions in the first 1 s. This is supported by Fig. 7b which shows that the number density of particles is higher with formulations 2 and 3 leading to higher probability of interparticle collisions when the particles are suspended in the air, allowing a better entrainment into the airstream. Higher collision numbers were obtained for model formulations 4–7. An increase in surface roughness on RMCCs led to an increase on the collision number. This observation is similar as reported (42). The presence of various levels of roughness denoted as protrusions and ridges may therefore allow air to be free to permeate through the powder. As a result, it is reasonable to consider that the airflow permeates through channels and

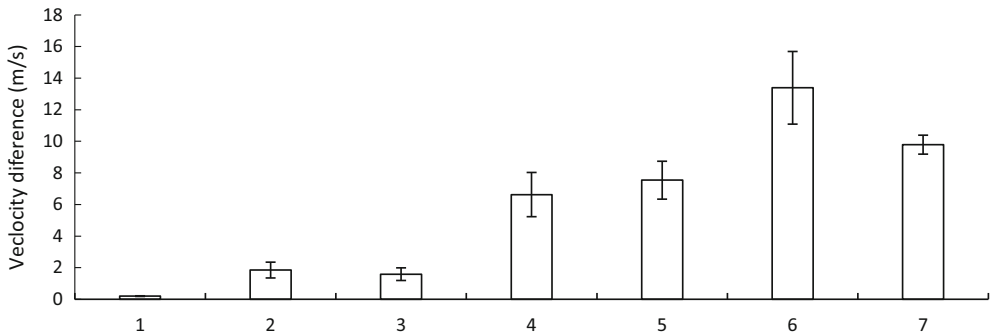

Fig. 10. Velocity difference of particles in the aerosolization chamber for different model formulations at 0.05 s of aerosolization in the chamber, $n = 10$

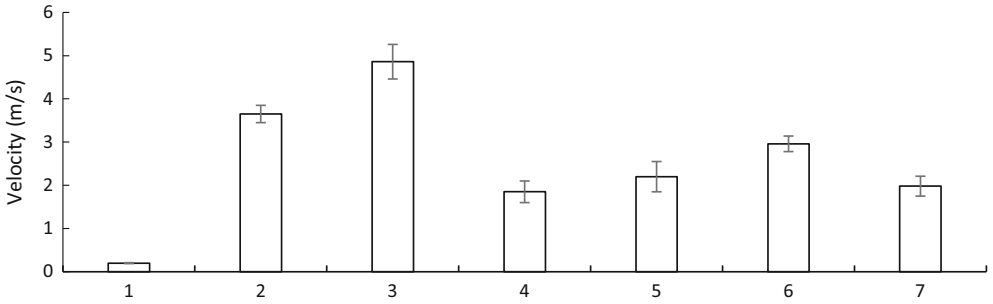

Fig. 11. Median velocity of model formulation at 0.5 s, $n = 10$

lifts the powder more easily. This leads to an increase in the number of particles above the powder bed and to a more frequent collision, reflected on a higher value of collision numbers. However, if a high concentration of particles with excessive surface roughness (Fig. 9, model formulation 7) is present, a drop in collision numbers was observed; thus, the advantage of roughness contribution to dispersibility by minimizing the points of contact seems to vanish and other mechanisms start taking over such as particle entrapment.

Collision is due to particle velocity differences (43). To further understand the collision process and collision number difference in different model formulations, it would be necessary to investigate the particle velocity difference. Particle velocity difference is defined in "Dry Powder Dispersion in Inhaler Chamber Real-Time Visualization." The particle velocity difference for different model formulations at 0.05 s is calculated and shown in Fig. 10. The velocity difference was the lowest for the MSS material. It might be because MSS moved slowly; hence, the velocity is generally low leading to a low velocity difference. Model formulations 2 and 3 had low velocity difference. This indicates that particles in model formulations 2 and 3 are more responsive to entrain into the airstream compared to the particles in the MSS formulation. It is possible that the velocity difference reflects the interfacial interactions influenced by the fluidization which in turn results in the generation of aerodynamic drag forces within the device.

With regard to particles with rougher surface (formulations 4–7), they showed higher velocity differences and more responsive to the air stream. A small portion of the particles are quickly accelerated when the rest of the particles are still in the powder bed. This creates a larger difference in particle's velocity, leading to wider velocity range. However, both the velocity (Fig. 11, formulation 4) and the portion of particles that can be accelerated are relatively low when the particle contains an overload of surface roughness (RMCC4). Furthermore, the velocity difference between particles dropped compared to the moderately rough particles. The results of the velocity difference support the fact that collisions occur due to high velocity heterogeneity. This finding agrees with the observation for collision numbers.

Particle Velocity and Velocity Change Due to Impact and Collision

Particle median velocity for the various model formulations is displayed in Fig. 11 where the median velocity is the 50th percentile of velocity plot. Figure 10 shows that the overall velocity difference observed in formulations 4–7 does not necessarily correspond to a high median velocity in Fig. 11. Model formulations 4–7 have particles with lower median velocity compared to those particles of formulations 2 and 3. Thus, the particles with rougher surfaces collide with each other more frequently as indicated by the higher collision numbers (Fig. 9). One explanation could be that more frequent collisions resulted in a homogenization of the velocity distribution causing the reduction of the median particle velocity.

Figure 12 displays the particle median velocity changes (Δv) for the model formulations. The MSS displayed smaller change due to its low velocity. The strong agglomerates formed by MSS, as evidenced by the low FPF, are difficult to disperse. Previous studies have suggested that powders that are difficult to fluidize lift as plugs, due to their adhesion and aerodynamic forces, and that may not entrain into the air stream as easily due to the elutriation behavior (27,42). It is suggested that the impact with other agglomerates or obstacle may paralyze the particles making the velocity change to be at their minimal. In contrast, Fig. 11 for model formulations 2

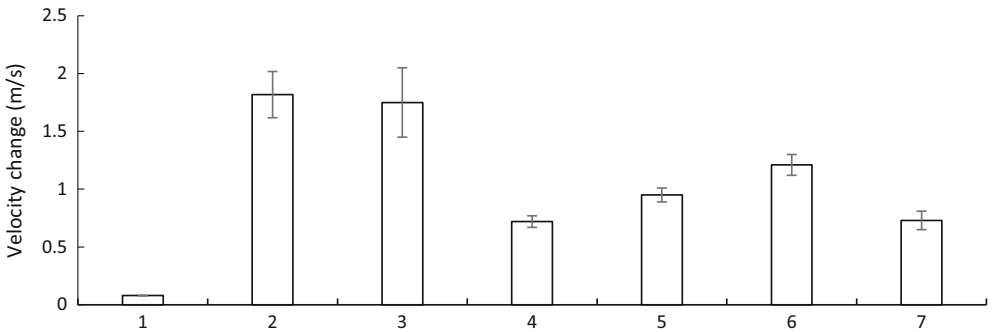

Fig. 12. Overall median velocity change after collision, $n = 10$

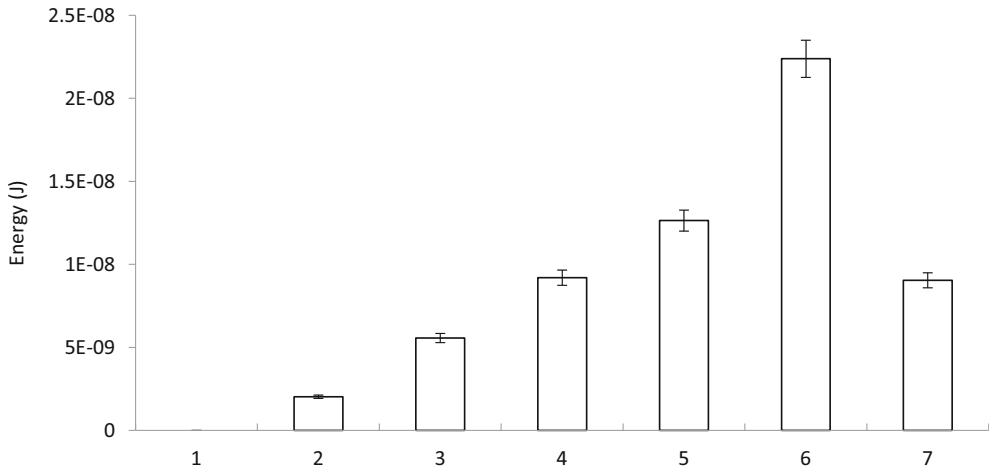

Fig. 13. Energy exchange for model formulations during collisions, $n = 10$

and 3 has relatively higher velocity before collision and a huge velocity change is observed for these two model formulations. Model formulations 4–7 have relatively low velocity change due to relatively low velocity. The low velocity for model formulations 4–7 is due to extensive collision, suggesting particle-obstacle impact and particle-particle collisions.

Energy Dissipation and FPF

As discussed in an earlier publication (39), it was found that powder dispersion was due to the drag force, collision, and impact. The impact/collision intensity and frequency are the main parameters governing particle dispersion (41). The combined effect of impact/collision intensity and frequency can be reflected by the energy dissipation during collision process (26) according to Eq. (1) in "Dry Powder Dispersion in Inhaler Chamber Real-Time Visualization." The results are plotted in Fig. 13. The energy exchange due to collision for MSS is very low. The model formulations 4–7 have higher energy exchange during collisions. The trend corresponds well with in vitro performance of the model formulations. A higher energy exchange during collisions leads to a better in vitro performance. The energy exchange due to collisions is only one of the factors governing dispersion. RMCCs can also be well-dispersed by drag force and collisions as shown in Fig. 7. Figure 13 only considers collisions, whereas in vitro performance in Fig. 6 is reflecting the combined effect of both drag forces and collisions. This study demonstrates the potential of the visualization approach of a dynamic process such as powder dispersion. Thus, a better insight of the dispersion mechanisms can be elucidated with the combined effect of the drag force and the collisions are considered.

CONCLUSION

The effect of surface roughness on dry powder dispersion has been investigated using visualization and image analysis techniques. Images of different model formulations composed of different carriers were captured. Carrier excipients with rougher surfaces can be dispersed and explained based on both by the drag force and the collisions. The tendency of having higher number of particles suspended in the air stream brings as a consequence higher collision numbers for a certain period of time. The combined effect of drag force and collisions results in better in vitro performance. This investigation also confirms that powder dispersion is a dynamic process; the approach proposed herein may be utilized as analytical tool along with FPF to predict the powder inhaler performance during powder dispersibility and entrainment tendencies. The recommendation is to analyze powder dispersibility from a dynamic perspective.

ACKNOWLEDGMENTS

The authors wish to thank for the partial support of this work to the Dane O. Kildsig Center for Pharmaceutical Research (CPPR) at Purdue University.

REFERENCES

1. Irngartinger M, Camuglia V, Damm M, Goede J, Frijlink HW. Pulmonary delivery of therapeutic peptides via dry powder inhalation: effects of micronisation and manufacturing. Eur J Pharm Biopharm. 2004;58(1):7–14.
2. Ibrahim BM, Jun SW, Lee MY, Kang SH, Yeo Y. Development of inhalable dry powder formulation of basic fibroblast growth factor. Int J Pharm. 2010;385(1–2):66–72.
3. Kou X, Chan LW, Steckel H, Heng PWS. Physico-chemical aspects of lactose for inhalation. Adv Drug Deliv Rev. 2012;64(3):220–32.
4. Kawashima Y, Serigano T, Hino T, Yamamoto H, Takeuchi H. Effect of surface morphology of carrier lactose on dry powder inhalation property of pranlukast hydrate. Int J Pharm. 1998;172(1–2):179–88.
5. Dickhoff BH, de Boer AH, Lambregts D, Frijlink HW. The interaction between carrier rugosity and carrier payload, and its effect on drug particle redispersion from adhesive mixtures during inhalation. Eur J Pharm Biopharm. 2005;59(1):197–205.
6. Dickhoff BH, de Boer AH, Lambregts D, Frijlink HW. The effect of carrier surface treatment on drug particle detachment from crystalline carriers in adhesive mixtures for inhalation. Int J Pharm. 2006;327(1–2):17–25.

7. Zeng XM, Martin GP, Marriott C, Pritchard J. The influence of carrier morphology on drug delivery by dry powder inhalers. Int J Pharm. 2000;200(1):93–106.
8. Iida K, Hayakawa Y, Okamoto H, Danjo K, Leuenberger H. Preparation of dry powder inhalation by surface treatment of lactose carrier particles. Chem Pharm Bull. 2003;51(1):1–5.
9. Monckedieck M, Kamplade J, Fakner P, Urbanetz NA, Walzel P, Steckel H, et al. Dry powder inhaler performance of spray dried mannitol with tailored surface morphologies as carrier and salbutamol sulphate. Int J Pharm. 2017;524(1–2):351–63.
10. Chan LW, Lim LT, Heng PW. Immobilization of fine particles on lactose carrier by precision coating and its effect on the performance of dry powder formulations. J Pharm Sci. 2003;92(5):975–84.
11. Kumon M, Yabe Y, Kasuya Y, Suzuki M, Kusai A, Yonemochi E, et al. Applicability of DPI formulations for novel neurokinin receptor antagonist. Int J Pharm. 2008;356(1–2):102–9.
12. Flament M-P, Leterme P, Gayot A. The influence of carrier roughness on adhesion, content uniformity and the in vitro deposition of terbutaline sulphate from dry powder inhalers. Int J Pharm. 2004;275(1–2):201–9.
13. de Boer AH, Hagedoorn P, Gjaltema D, Goede J, Kussendrager KD, Frijlink HW. Air classifier technology (ACT) in dry powder inhalation Part 2. The effect of lactose carrier surface properties on the drug-to-carrier interaction in adhesive mixtures for inhalation. Int J Pharm. 2003;260(2):201–16.
14. Kaialy W, Martin GP, Larhrib H, Ticehurst MD, Kolosionek E, Nokhodchi A. The influence of physical properties and morphology of crystallised lactose on delivery of salbutamol sulphate from dry powder inhalers. Colloids Surf B. 2012;89:29–39.
15. Young P, Kwok P, Adi H, Chan H-K, Traini D. Lactose composite carriers for respiratory delivery. Pharm Res. 2009;26(4):802–10.
16. Kaialy W, Ticehurst MD, Murphy J, Nokhodchi A. Improved aerosolization performance of salbutamol sulfate formulated with lactose crystallized from binary mixtures of ethanol—acetone. J Pharm Sci. 2011;100(7):2665–84.
17. Adi S, Adi H, Tang P, Traini D, H-k C, Young PM. Micro-particle corrugation, adhesion and inhalation aerosol efficiency. Eur J Pharm Sci. 2008;35(1–2):12–8.
18. Littringer EM, Mescher A, Schroettner H, Achelis L, Walzel P, Urbanetz NA. Spray dried mannitol carrier particles with tailored surface properties - the influence of carrier surface roughness and shape. Eur J Pharm Biopharm. 2012;82(1):194–204.
19. Kaialy W, Ticehurst M, Nokhodchi A. Dry powder inhalers: mechanistic evaluation of lactose formulations containing salbutamol sulphate. Int J Pharm. 2012;423(2):184–94.
20. Paajanen M, Katainen J, Raula J, Kauppinen EI, Lahtinen J. Direct evidence on reduced adhesion of salbutamol sulphate particles due to L-leucine coating. Powder Technol. 2009;192(1):6–11.
21. Adi H, Traini D, Chan H-K, Young PM. The influence of drug morphology on aerosolisation efficiency of dry powder inhaler formulations. J Pharm Sci. 2008;97(7):2780–8.
22. Kaialy W, Larhrib H, Ticehurst M, Nokhodchi A. Influence of batch cooling crystallization on mannitol physical properties and drug dispersion from dry powder inhalers. Cryst Growth Des. 2012;12(6):3006–17.
23. Podczeck F. The influence of particle size distribution and surface roughness of carrier particles on the in vitro properties of dry powder inhalations. Aerosol Sci Technol. 1999;31(4):301–21.
24. Podczeck F. The relationship between physical properties of lactose monohydrate and the aerodynamic behaviour of adhered drug particles. Int J Pharm. 1998;160(1):119–30.
25. Voss A, Finlay WH. Deagglomeration of dry powder pharmaceutical aerosols. Int J Pharm. 2002;248(1–2):39–50.
26. de Boer AH, Hagedoorn P, Gjaltema D, Goede J, Frijlink HW. Air classifier technology (ACT) in dry powder inhalation: part 1. Introduction of a novel force distribution concept (FDC) explaining the performance of a basic air classifier on adhesive mixtures. Int J Pharm. 2003;260(2):187–200.
27. Donovan MJ, Kim SH, Raman V, Smyth HD. Dry powder inhaler device influence on carrier particle performance. J Pharm Sci. 2012;101(3):1097–107.
28. Donovan MJ, Smyth HDC. Influence of size and surface roughness of large lactose carrier particles in dry powder inhaler formulations. Int J Pharm. 2010;402:1–2):1–9.
29. Saint-Lorant G, Leterme P, Gayot A, Flament MP. Influence of carrier on the performance of dry powder inhalers. Int J Pharm. 2007;334(1–2):85–91.
30. Adi H, Larson I, Stewart P. Laser diffraction particle sizing of cohesive lactose powders. Powder Technol. 2007;179(1–2):90–4.
31. Schultz J, Lavielle L, Martin C. The role of the interface in carbon-fiber epoxy composites. J Adhes. 1987;23:45–60.
32. Marple VA, Olson BA, Santhanakrishnan K, Mitchell JP, Murray SH, Hudson-Curtis BL. Next Generation Pharmaceutical Impactor (A New Impactor for Pharmaceutical Inhaler Testing). Part II: Archival Calibration. J Aerosol Med. 2004;16(3):301–24.
33. Kaialy W, Martin GP, Ticehurst MD, Royall P, Mohammad MA, Murphy J, et al. Characterisation and deposition studies of recrystallised lactose from binary mixtures of ethanol/butanol for improved drug delivery from dry powder inhalers. AAPS J. 2011;13(1):30–43.
34. Peters HJW. Lactose for direct compressions. Chem Week. 2009;22:197–8.
35. Wong DYT, Wright P, Aulton ME. The deformation of alpha-lactose monohydrate and anhydrous alpha-lactose monocrystals. Drug Dev Ind Pharm. 1988;14(15–17):2109–26.
36. Cline D, Dalby R. Predicting the quality of powders for inhalation from surface energy and area. Pharm Res. 2002;19(9):1274–7.
37. Boraey MA, Hoe S, Sharif H, Miller DP, Lechuga-Ballesteros D, Vehring R. Improvement of the dispersibility of spray-dried budesonide powders using leucine in an ethanol-water cosolvent system. Powder Technol. 2013;236:171–8.
38. Kinnunen H, Hebbink G, Peters H, Huck D, Makein L, Price R. Extrinsic lactose fines improve dry powder inhaler formulation performance of a cohesive batch of budesonide via agglomerate formation and consequential co-deposition. Int J Pharm. 2015;478(1):53–9.
39. Kou X, Wereley ST, Heng PWS, Chan LW, Carvajal MT. Powder dispersion mechanisms within a dry powder inhaler using microscale particle image velocimetry. Int J Pharm. 2016;514(2):445–55.
40. Podczeck F, Newton JM, James MB. The estimation of the true area of contact between microscopic particles and a flat surface in adhesion contact. J Appl Phys. 1996;79(3):1458–63.
41. Chen L, Heng R-L, Delele MA, Cai J, Du D-Z, Opara UL. Investigation of dry powder aerosolization mechanisms in different channel designs. Int J Pharm. 2013;457(1):143–9.
42. Sommerfeld M. Analysis of collision effects for turbulent gas-particle flow in a horizontal channel: part I. Particle transport. Int J Multiphase Flow. 2003;29(4):675–99.
43. Goswami PS, Kumaran V. Particle dynamics in a turbulent particle-gas suspension at high Stokes number. Part 1. Velocity and acceleration distributions. J Fluid Mech. 2010;646:59–90.